# Power Fluctuations In High Installation Density Offshore Wind Fleets

Juan Pablo Murcia Leon[1], Matti Juhani Koivisto[1], Poul Sørensen[1], and Philippe Magnant[2]

[1]Department of Wind Energy, Technical University of Denmark, 4000 Roskilde, Denmark
[2]Elia Asset, Boulevard de l'Empereur 20, 1000 Bruxelles

**Correspondence:** Juan Pablo Murcia (jumu@dtu.dk)

**Abstract.**

Detailed simulation of wind generation as driven by weather patterns is required to quantify the impact on the electrical grid of the power fluctuations in offshore wind power fleets. This paper focuses on studying the power fluctuations of high installation density offshore fleets since they present a growing challenge to the operation and planning of power systems in Europe. The Belgian offshore fleet is studied because it has the highest density of installation in Europe by 2020 and a new extension is expected to be fully operational by 2028. Different stages of the future installed capacity, turbine technology, and turbine storm shutdown technologies are examined and compared. This paper analyzes the distribution of power fluctuations both overall and during high wind speeds. The simulations presented in this paper use a new t-student distributed wind speed fluctuations model that captures the missing spectra from the weather reanalysis-simulations. An updated plant storm shutdown model captures the plant behaviour of modern high wind speed turbine operation. Detailed wake modeling is carried out using a calibrated engineering wake model to capture the Belgium offshore fleet and its tight farm to farm spacing. Long generation time series based on 37 years of historical weather data in 5 $\mathrm{min}$ resolution are simulated to quantify the extreme fleet-level power fluctuations. The model validation with respect to the operational data of the 2018 fleet shows that the methodology presented in this paper can capture the distribution of wind power and its spatio-temporal characteristics. The results show that the standardized generation ramps are expected to be reduced towards the 4.4 $\mathrm{GW}$ of installations due to the larger distances between plants. The most extreme power fluctuations occur during high wind speeds, with large down-ramps occurring in extreme storm events. Extreme down-ramps are mitigated using modern turbine storm shutdown technologies, while extreme up-ramps can be mitigated by the system operator. Extreme ramping events also occur at below-rated wind speeds, but mitigation of such ramping events remains a challenge for transmission system operators.

## 1 Introduction

Belgium has adopted the target of a 65% reduction of greenhouse gases emission levels by 2050, a less ambitious target than the European target of 80% by 2050. Nevertheless, Belgium is expected to increase the share of renewable energy sources, with an expected increase of wind energy share of between 37% to 44% by 2050 (Mikova et al., 2019). Belgian offshore wind power fleet will be, by the end of 2020, one of the areas with the highest installation density in the North Sea (approximately

10 $\mathrm{MW/km^2}$, while the average is 6.6 $\mathrm{MW/km^2}$), with an installed capacity of circa 2.3 GW over a marine area of circa 225 $\mathrm{km^2}$ in the proximity to the Netherlands. Furthermore, the planned expansion of the Belgian offshore fleet will bring the capacity up to between 4.0 and 4.4 GW by 2028 (Elia, 2019, 2017). Previous studies of the impact of the Belgian offshore fleet in its energy system exist: (Elia, 2018) studies the impact of storm and ramping events on the system imbalances, while (Buijs et al., 2009) investigates the required investment by the Belgium power system for integrating the 2.3 GW of offshore wind.

Geographical smoothing of the fleet-wise offshore wind production is expected in the 4.4 GW scenario as the new plants are located further apart from the existing fleet and due to the decrease of correlation between power productions from plants further apart. Several studies explore the effects of the distance among wind power plants in the fleet/portfolio wind production such as: (Santos-Alamillos et al., 2017; Tejeda et al., 2018; Roques et al., 2010; Koivisto et al., 2016). Additionally, the expected increase in rotor diameter, hub height and general improvements of wind turbine technology can have a smoothing effect in fleet-wise wind power production (Koivisto et al., 2019b).

The distribution of the fleet-level power fluctuations is necessary to understand and model the impact of the future expansions of the Belgian offshore fleet into the Belgian energy system (Huber et al., 2014). (Holttinen et al., 2011) present a detailed analysis of the impacts of large amounts of wind power on the design and operation of power systems. (Holttinen et al., 2016) shows that characteristics of variability and uncertainty of wind power are an important input for wind integration studies, with impacts, e.g., on system balancing and grid reinforcing needs. A long term dynamical simulation of the offshore wind power generation is required to assess the impact of the extreme power fluctuations in the energy system (Pfenninger, 2017).

The purpose of this paper is to quantify the distribution of ramp rates as a measure for power fluctuations when extending the offshore wind capacity in Belgium. This research proposes a methodology for simulating wind power production time series and performing a validation using operational measurements on the 2018 fleet. This paper concentrates on the simulations of the time series of offshore wind generation for several scenarios. The simulated time series can be used as inputs in power and energy system impact analyses, but a detailed model of the energy system is not in scope. The hypothesis of this study is that power fluctuations in the Belgian offshore wind fleet will be reduced by a combination of increase spatial smoothing (larger distances between new installations) and the use of turbines with controlled high wind speed operation.

This paper includes several novel methodologies that addresses current gaps in large scale offshore wind generation simulation: first, it presents a t-student distributed wind speed fluctuations model and its validation. This model is based on the work by (Mehrens et al., 2016) that shows that wind speed fluctuations are non-Gaussian, and by (Koivisto et al., 2016) that models the error terms in a multivariate autoregressive model with a marginally t-student distributed Gaussian copula. Second, this paper presents an update to the hysteresis plant storm shutdown model by (Litong-Palima et al., 2016) and its validation. Third, the methodology for simulating power production takes into account wake losses including farm to farm interactions. Fourth, a detailed validation of the results in terms of capacity factors (CF), high wind speed operation, power fluctuations and spatial-correlations for the existing fleet demonstrates the simulation capability of the model chain used. Additionally, this paper has practical significance because it illustrates how the proposed methodology can be used to accurately predict the distribution of the fleet-level power fluctuations including its most severe extremes.

## 2 Literature Synthesis

Large energy system modeling is required in order to design, plan, and adapt to, the future transition to greener technologies. (Pfenninger et al., 2014) presents a literature review on large energy system models and identifies the main challenges of large energy system simulations as: (a) temporal/spacial resolution, (b) uncertainty and transparency, (c) growing complexity of interconnected energy systems with diverse mixture of technologies (d) integrating the impact of policy and other human behaviours. Furthermore, (Engeland et al., 2017) present a review of the modeling approaches for variable renewable energy (VRE, i.e. wind and solar). This review highlights the different methodologies required to simulate the generation of a wind power fleet as a time series. (Holttinen et al., 2016) highlight the importance of modeling geographical smoothing when analyzing variability and uncertainty of wind power in system integration studies. The most common approaches are: (1) stochastic time series simulations, (2) simulations based on meteorological reanalysis-simulations, and (3) combinations of them.

Stochastic time series simulation of fleet-level wind power production has been used in several studies. (Ekström et al., 2017), (Koivisto et al., 2016), (Klöckl and Papaefthymiou, 2010) and (Olauson et al., 2017) are examples of applications and implementations of extended vector autoregressive models to simulate VRE generation time series. (Sørensen et al., 2002) introduced the use of a stochastic time series model for simulating the wind speed fluctuations by combining the Kaimal turbulent spectra (for fluctuations within 10- $\mathrm{min}$ resolutions) with a low frequency spectra designed to simulate the weather patterns in larger scale fluctuations. All these simulation approaches rely on stochastic time series models to capture the auto- and cross-correlations of the power time series on multiple locations. Some of these stochastic models are fitted on measured historical data, and have the limitation of not being able to predict the production time series on wind power fleets with different characteristics (i.e. installed capacity, locations, turbine types) from the original data. Direct stochastic power simulations have the advantage of not requiring the simulation of wind speeds, but instead rely on empirical transformations of the data to correct for the non-stationarity, non-Gaussianity and correlation structure of power fluctuations. (Fertig, 2019) introduces an empirical model to apply stochastic models to different installed capacity and locations.

Weather driven wind power time series generation simulations consists in modelling the wind production as driven by wind speed time series obtained from: (1) meteorological reanalysis datasets such as: ERA-interim (Dee et al., 2011), MERRA (Gelaro et al., 2017) or ERA-5 (Hersbach et al., 2020); (2) weather research and forecasting (WRF) model simulations (Skamarock et al., 2008). Example applications of weather driven wind generation simulations can be read in: (Nuño et al., 2018; Olauson and Bergkvist, 2015; Marinelli et al., 2014; Leahy and Foley, 2012; Von Bremen, 2010; Staffell and Pfenninger, 2016; Thomaidis et al., 2016; Staffell and Pfenninger, 2018). The main advantages of using meso-scale weather driven generation simulations are: (a) the simulations rely on the predictions of wind speeds and wind directions, among other meteorological parameters, and therefore have physical consistency between different locations/times. (b) The simulations can be performed on any combination of installed capacity, locations, wind turbine technologies. (c) The simulations can be extended to cover larger periods of time, which will be necessary for reliability or extreme event probability estimations, (Pfenninger, 2017). The disadvantages are: (a) low spatio-temporal resolution means that not all the variability in the wind speed is captured. Hourly

resolution is widely used in most studies, but simulations can be carried out with 10 $\mathrm{min}$ resolutions or more but with a significant additional computational costs (Liu et al., 2011; Talbot et al., 2012). Spatial resolution of 10 $\mathrm{km}$ is widely used in wind energy (González-Aparicio et al., 2017), but WRF simulations can be performed in up to 100m x 100m (Liu et al., 2011; Talbot et al., 2012), while modern reanalysis datasets have resolutions between 10-75 km, (González-Aparicio et al., 2017; Olauson, 2018). (b) Simulated time series are smoother than measurements because the weather models tend to filter the high frequency oscillations from the signals in order to ensure convergence. (c) Due to the coarse temporal resolution turbulence spectra is missing; which is necessary to simulate with higher resolutions than 10 $\mathrm{min}$.

Stochastic models are designed to capture the missing wind speed fluctuations. (Veers, 1988) demonstrated that time series interpolated from a grid of correlated time series produce a decrease in the apparent spectra, and proposed a methodology to add missing fluctuations to compensate for this effect. (Larsén et al., 2012) reports the missing spectra in WRF with respect to measurements and analyses the implications to extreme wind speed estimation. (Larsén and Kruger, 2014) introduce and apply the spectral correction for WRF in South Africa, while (Sørensen et al., 2018) apply it in the 2025 wind power scenario in South Africa. (Koivisto et al., 2020) calibrates the parameters of the stochastic wind speed fluctuations model based on measurements. (Mehrens et al., 2016) presents non Gaussian distribution of wind speed fluctuations in WRF and in measurements in offshore met masts sites. (Olauson et al., 2016) presents an empirical approach to model the fluctuations by introducing a machine learning regression model for the volatility and optimizing the phase angles between the different Fourier modes of the fluctuations to capture auto- and cross-correlations. For reference, (Liu et al., 2017; Kiviluoma et al., 2016; Apt, 2007) present modern experimental spectra of wind power generation.

The wake behind the turbine is a flow characterized by a decrease on the mean wind speed and an increase on the turbulence downstream. (Porté-Agel et al., 2020) provides a review of the work on the wake modeling and measuring field. In summary, the wakes translate into a lower power production on turbines operating on the wake of other turbines. Wind turbine wakes recover as a function of the distance from the turbine which causes the effect to be most important when turbines are closely spaced. As turbines in the Belgian fleet are tightly spaced, significant wake effects are expected.

Farm wake is the aggregated effect of the wakes from all the turbines in a farm to the turbines in a nearby farm. Such effects have been reported to retain wind speed deficits of up to $2\%$ at downstream distances between 20-60 km (Volker et al., 2017). This distance of expected influence of farm wakes depends on the plant size, number of turbines and on the atmospheric boundary layer stability (Porté-Agel et al., 2020). Farm effects are important in this study because of the proximity between the offshore wind plants in the Belgian waters.

(Agora Energiewende et al., 2020) and (Volker et al., 2017) report an expected capacity factor of around 30%-50% for areas with high power density (10 MW/km$^2$) spreading over areas between 1-10 km$^2$, depending on the wind resource on the region. Note that these capacity factors include the intra-farm (wakes of turbines in the same farm) and farm-to-farm wake losses.

## 3 Methods

### 3.1 Future wind turbine technology and installed capacity scenarios

To build representative scenarios for 2025-2028, the trends in offshore turbine technology are analyzed in terms of turbine capacity, specific power (ratio between rated power and rotor area) and hub height, see Fig. 1. The trends combine the current turbines installed or planned in Belgium and the Netherlands, the technology projections (Danish Energy Agency, 2020), and the commercial wind turbine prototype information available on the main wind turbine manufacturer's websites. Fig. 1 shows that there is a linear trend in increasing hub height and turbine capacity, while the specific power tends to follow a cyclic trend with linear increase followed by a drop in specific power. Two turbine technology scenarios are propose in this paper (Tech A and Tech B), both scenarios assume the same rated power but different specific power. Tech A turbine has a high specific power, while Tech B has low specific power. The range of difference in rated power from different manufacturers is expect not to have significant impact on the results presented in this paper.

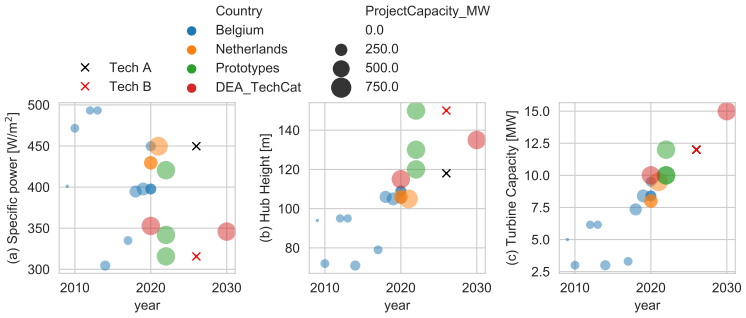


**Figure 1.** Trends in specific power, hub height and turbine capacity for offshore turbines.

The power curves from the two turbine technologies are approximated based on the specific power, using the power and thrust coefficient curves of large rotors in DTU Wind Energy's database. Modern wind turbines are offered with high wind speed operation, which consists in extending the cut-off wind speed and implementing different control strategies to reduce the aeroelastic loads on the turbine components and hence reduce the power production. In this study a generic high wind speed operation technology (HWS Deep) is compared with respect the traditional cut-off wind speed at 25 $\mathrm{ms}^{-1}$, see Fig. 2. The HWS deep type represents modern turbines designed to continue operation at high wind speeds and mitigate the ramping due to storm shutdowns. High wind speed operation technology is commercially available, but every manufacturer uses a different control strategy which results in differences in the power curves at high wind. The HWS power curve presented in Fig. 2 is proposed to have manufacturer agnostic HWS technology model. In this paper there are four turbine-curtailment technology scenarios: Tech A with 25 direct cut-off, Tech A with HWS Deep, Tech B with 25 direct cut-off, and Tech B with HWS Deep.

Future installation development is split into three scenarios or stages: BE2018 with 0.9 GW represents the validation dataset in which four years of operational data is available, BE 2.3 GW consists of the plants in BE2018 and the plants to be com-

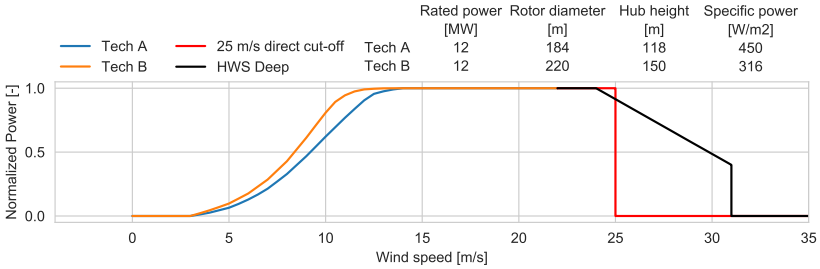


**Figure 2.** Power curves and technical parameters for assumed technology and storm shutdown scenarios.

missioned by 2020, BE 4.4 GW consists of the plants in BE 2.3 GW and future extension, see Fig. 3 and table 1. The turbine and layout used in the plants in BE 2.3 GW scenario are known (Sørensen et al., 2020). The BE 4.4 GW scenario is studied by varying the turbine and shutdown technology for the additional 2.1 GW of installations. The plant layout in BE 4.4 GW is generated by maximizing the spacing between the turbines needed to reach the full installed capacity. Furthermore, the offshore fleet in the Netherlands (1.5 GW to start operating by 2020) is also modelled in the BE 2.3 GW and 4.4 GW scenarios because of its proximity .

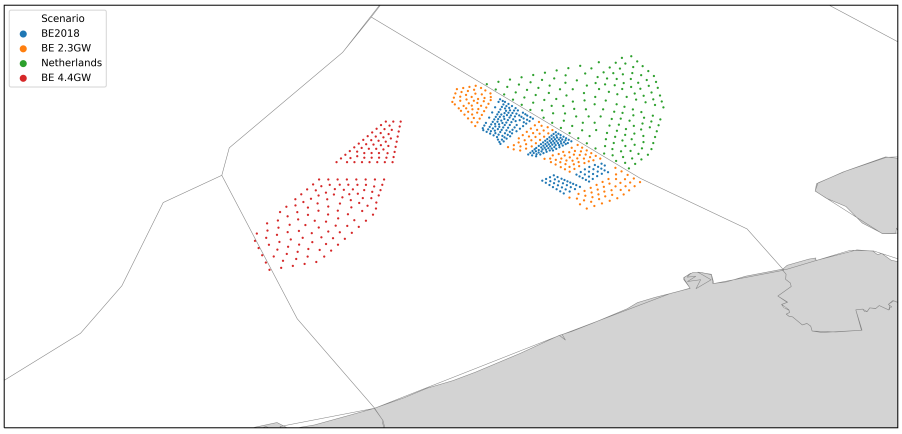


**Figure 3.** Plant and turbine locations for the different stages of offshore wind installations.

### 3.2 Modeling

This section describes all the methodology used to produce the power time series simulations, including wake modeling, wind speed time series generation and wind plant storm shutdown modeling implemented in CorRES (correlations in renewable energy sources) (Koivisto et al., 2019a, 2020). CorRES uses meso-scale weather driven renewable energy generation and has three sub-models: (1) meso-scale weather data and interpolation, (2) wind speed fluctuations model and (3) wind-to-power model which includes wake modelling and dynamic storm shut-down model.

| Scenario | Total Capacity GW | Turbine Capacity MW | Rotor Diameter m | Specific Power W/m2 | Hub Height m | Cut-off Tech |
|---|---|---|---|---|---|---|
| BE2018 | 0.9 | 3 to 6.15 | 90 to 126 | 305 to 493 | 72 to 95 | Direct 25 or 30 m/s |
| BE 2.3 GW | 2.3 | 7.25 to 9.5 | 154 to 164 | 395 to 450 | 105 to 109 | HWS Deep |
| Netherlands | 1.5 | 8 to 9.5 | 154 to 164 | 430 to 450 | 105 to 106 | HWS Deep |
| BE 4.4 GW Tech A 25 direct cut off | 4.4 | 12 | 184 | 450 | 118 | Direct 25 m/s |
| BE 4.4 GW Tech A HWS Deep | 4.4 | 12 | 184 | 450 | 118 | HWS Deep |
| BE 4.4 GW Tech B 25 direct cut off | 4.4 | 12 | 220 | 318 | 150 | Direct 25 m/s |
| BE 4.4 GW Tech B HWS Deep | 4.4 | 12 | 220 | 318 | 150 | HWS Deep |

**Table 1.** Plant and turbine characteristics for the different stages of offshore wind installations. Characteristics are given for the added turbines with respect the previous stage of installation except for total capacity. The Dutch plants are taken into account when modelling external wake impacts on the Belgian fleet. Note that the actual turbines and plant layouts for BE2018, BE 2.3 GW and Netherlands scenarios were used.

### 3.2.1 Wind speed time series simulation

Wind speed time series on multiple locations are simulated by combining a pre-computed database of meteorological reanalysis simulations ($u_{\text{WRF}}$) and a stochastic model to compensate for the missing fluctuations ($\delta_u$), see Eq. (1), where $x_j$ is the location of plant $j$ at a given time, $t$. The following methodology is based on (Sørensen et al., 2008) and (Koivisto et al., 2020).

$$u(x_j,t) = u_{\text{WRF}}(x_j,t) + \delta_u(x_j,t) \tag{1}$$

CorRES meteorological reanalysis data is obtained running WRF (Skamarock et al., 2008) to downscale the ERA-Interim reanalysis data (Dee et al., 2011) in a 10 km x 10km x 1 h resolution. (Nuño et al., 2018) give a detailed description of the WRF simulations used in this paper. The model results are stored on multiple heights above ground (50,80,100,120,150). Linear interpolation in horizontal coordinates and piece wise power law interpolation is used to obtain the time series on a given farm center position.

The stochastic model used to compensate the missing high frequency spectra and the turbulence contribution to the inter-timestep variability in the wind speed signals is characterized by its power spectral density (PSD), $S_{jj}(f)$, see Eq. (2). In this equation the coefficient $a_1$ is a parameter of the spectra, while $f_0$ controls the lower frequency from which variability will be added. (Koivisto et al., 2020) reports the calibration of $a_1$ and $f_0$ to wind speed measurements in Høsøre, Risø and Cabauw.

The fluctuations spectra is designed to capture the full range spectra as reported by (Larsén et al., 2016) with the addition of the $f_0$ parameter, used to minimize the low frequency modification of the WRF time series.

$$S_{jj}(f) = \frac{a_1}{f_0^{5/3} + f^{5/3}} \tag{2}$$

Since the simulations represent several locations, the coherence between the wind speed fluctuations (on a given frequency) between two locations is specified by the coherence function, $\gamma_{jk}(f)$, in Eq. (3). Where $A_{jk}$ is the decay coefficient, $d_{jk}$ is the distance between the locations, $u_{jk}$ is the mean wind speed on the locations.

$$\gamma_{jk}(f) = e^{-A_{jk} d_{jk} f / u_{jk}} \tag{3}$$

The decay coefficient is defined as a function the streamwise ($A_s$) and transversal ($A_t$) components in Eq. (4), by projecting them along the direction of locations-alignment, $\alpha_{jk}$ is the direction of alignment and $\theta_{jk}$ is the mean wind direction in the locations. (Sørensen et al., 2008) reports calibrated values of $A_t = 4$ and $A_s = u_{jk}/2$ based on multiple location measurements in Høsøre.

$$A_{jk} = \sqrt{\left(A_s \cos(\theta_{jk} - 270 - \alpha_{jk})\right)^2 + \left(A_t \sin(\theta_{jk} - 270 - \alpha_{jk})\right)^2} \tag{4}$$

The spectral matrix, $\mathbf{S}$, is computed using the cross-spectra and coherence functions on a discretized frequency bin (with center frequency $f_m$), for every pair of location $j$ and $k$, see Eq. (5).

$$\mathbf{S}_{jk}(f_m) = \gamma_{jk}(f_m) \sqrt{S_{jj}(f_m) S_{kk}(f_m)} \tag{5}$$

The time series generation methodology presented in (Veers, 1988) is used. The spectral matrix is approximated by a real, lower triangular matrix $\mathbf{H}$, such that $\mathbf{S}(f_m) = \mathbf{H}(f_m)\mathbf{H}^T(f_m)$. This matrix is computed in an iterative manner following Eq. (6).

$$\mathbf{H}_{jk}(f_m) = \begin{cases} \left(\mathbf{S}_{jk}(f_m) - \sum_{l=1}^{k-1} \mathbf{H}_{jl}(f_m)\mathbf{H}_{kl}(f_m)\right)^{1/2} & \text{if } j = k \\ \left(\mathbf{S}_{jk}(f_m) - \sum_{l=1}^{k-1} \mathbf{H}_{jl}(f_m)\mathbf{H}_{kl}(f_m)\right) / \mathbf{H}_{jk}(f_m) & \text{if } j < k \end{cases} \tag{6}$$

Finally, the complex Fourier coefficients of the wind speed fluctuations, $V_j(f_m)$, are computed as a linear combination of the weights given by $\mathbf{H}(f_m)$ and a series of independent, unit-magnitude, white noise signals with random phases $\phi_{km}$ uniformly distributed on the interval $(0, 2\pi)$, see Eq. (7). The Gaussian-process time series, $V_j(t)$, are obtained by applying an inverse Fourier transformation.

$$V_j(f_m) = \sum_{k=1}^{j} \mathbf{H}_{jk}(f_m)\, e^{i\phi_{km}} \tag{7}$$

In the present work the wind speed fluctuations are transformed using an iso-probability transformation to a truncated t-student marginally distributed Gaussian-copula, see Eq. (8). This transformation consist in transforming the Gaussian distributed fluctuations to the uniform space, using their cumulative density function, $F_{N,j}$, and then apply the inverse cumulative density function of the truncated t-distributed Gaussian-copula, $F^{-1}_{t,\upsilon,\tau,j}$. The degree of freedom of the t-student marginals, $\upsilon$, and the degree of truncation, $\tau$, are unique and the same for all plants, and are calibrated based on the measured wind speed fluctuations. Truncation of the t-student distribution is applied in order to match the extreme fluctuations seen on the wind speed measurements.

$$\delta_{u,j}(t) = F^{-1}_{t,\upsilon,\tau,j}(F_{N,j}(V_j(t))) \tag{8}$$

A simplified model for correcting the extreme wind speed events, $u = g(u) \times u$, is described in Eq. (9). This correction does not affect wind speeds lower than $20\ \mathrm{ms}^{-1}$ , while it applies a linearly growing factor for wind speeds above, with a maximum factor of $1.08$ for wind speeds above $26\ \mathrm{ms}^{-1}$ . This correction is based on the validation study of extreme wind speeds by (Bastine et al., 2018) and the measured wind speeds from existing offshore wind power plants in Belgium.

$$g(u) = \begin{cases} 1 & \text{if } u <= 20 \\ 0.08(u-20)/6 + 1 & \text{if } 20 < u < 26 \\ 1.08 & \text{if } u >= 26 \end{cases} \tag{9}$$

### 3.2.2 Wake Modeling

Wake effects are modelled using the engineering wake model proposed in (Bastankhah and Porté-Agel, 2014). This wake model consists of self-similar Gaussian wind speed deficits in Eq. (10), a linear wake expansion in Eq. (11), and energy deficit superposition in Eq. (12). In these equations $\Delta u$ is the wind speed deficit downstream, $u_\infty$ is the undisturbed wind speed, $C_T$ is the thrust coefficient, $\sigma$ is the wake width, $k$ is the wake expansion coefficient, $D$ is the rotor diameter, $(x, r)$ is the location where the deficit is to be evaluated in wake coordinates, while $N$ is the number of wind turbines in the farm.

$$\frac{\Delta u}{u_\infty} = \left(1 - \sqrt{1 - \frac{C_T}{8(\sigma/D)^2}}\right) \exp\left(-\frac{r^2}{2\sigma^2}\right) \tag{10}$$

$$\frac{\sigma}{D} = k\frac{x}{D} + 0.2\left(\frac{1+\sqrt{1-C_T}}{2\sqrt{1-C_T}}\right) \tag{11}$$

$$u = u_\infty - \sqrt{\sum_{m=1}^{N} \Delta u_m^2} \tag{12}$$

This model is used because of its simplicity and because it has been formulated to hold mass and momentum conservation equations in the wake flow behind a turbine, see (Porté-Agel et al., 2020).

The wake model is used to generate a plant power curve by simulating the power outcome of the plant as a function of the undisturbed mean wind speed and mean wind direction, $P(u, \theta)$. The wake model is evaluated including all turbines from neighboring farms, therefore it includes both intra-farm and farm-to-farm wakes. The resolution of the wake modelling is 1 degree in wind direction and 0.5 $\mathrm{ms}^{-1}$ in wind speeds. The plant power curve is interpolated on each time stamp of the wind speed and wind directions time series, ensuring the 360-degree periodicity on the wind direction. A simplified wake model calibration is performed to determine the wake expansion parameter that better fits the measured capacity factors in the BE2018 fleet.

### 3.2.3 Wind turbine/plant storm shutdown

Wind turbine storm shutdown operation consists in four different wind speed set points that specify the mean wind speed shutdown limits for 10 $\mathrm{min}$, 30 $\mathrm{s}$ and 1 $\mathrm{s}$ windows ($u_{600}$, $u_{30}$ and $u_1$). The turbine goes into shutdown if the wind speed moving average on a period is larger than its limit, for periods of $600, 30, 1$ seconds. The turbine only goes back to operation when the 10 $\mathrm{min}$ moving average wind speed is lower that the restart wind speed. In the present work modern turbine high wind speed operation (HWS Deep) is modelled with a linear decrease of power and different shutdown wind speed set points. Fig. 4 shows the single turbine storm shutdown for the 25 $\mathrm{m/s}$ direct cut-off and the HWS deep technologies.

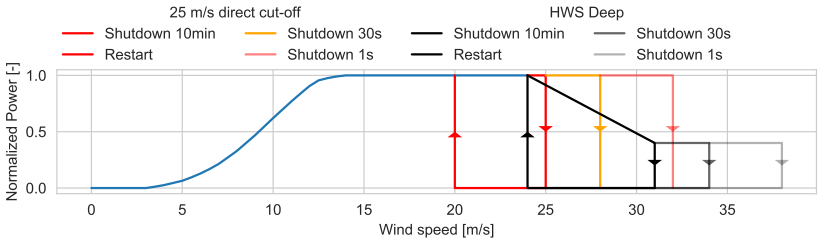


**Figure 4.** Single turbine storm shutdown for the three high wind speed operation technologies.

Wind farm storm shutdown behaviour is different from the individual turbine shutdown: in a wind farm not all the turbines will shutdown at exactly the same time because the wind speed fluctuations in each turbine are different, which means that each turbine has a different wind speed time series that reaches shutdown at different times. (Macdonald et al., 2014) studies the high wind speed shutdowns behaviour of two wind farms in Great Britain. Plant shutdown is characterized by discrete levels of reduced capacity operation, each level representing the power curve for the plant when a number of turbines are off. The wind farm storm shutdown hysteresis model presented in (Litong-Palima et al., 2016) is extended to model the plant-level operation of turbines with modern high wind speed operation. The hysteresis model consists of a simple algorithm that forces the power to move proportionally along the power curve unless the wind speed reaches the restart or shutdown curves, see Fig. 4. The

turbine-level storm shutdown is thus first transformed to plant-level behaviour based on simulating a set of storm cases on high resolution on turbine-level generic plant.

CorRES allows modelling a wind power plant as both multiple-turbines and plant-level. However, the large scale simulations of the entire fleet are computationally feasible only on plant-level. Plant simulations with individual turbine storm shutdown simulations are carried out for 15 historical high wind speed days (in which max wind speed is larger 20 $\mathrm{ms}^{-1}$ in the WRF data) in 1s resolution. These simulations are used to define the plant power curve, the restart line and the shutdown line, see Fig. 5. In this Fig. it can be observed that the high wind speed operation part of the plant power curve differs from the piece-wise linear behavior of the individual turbine, which is a consequence of the difference between the wind speed fluctuations on each turbine.

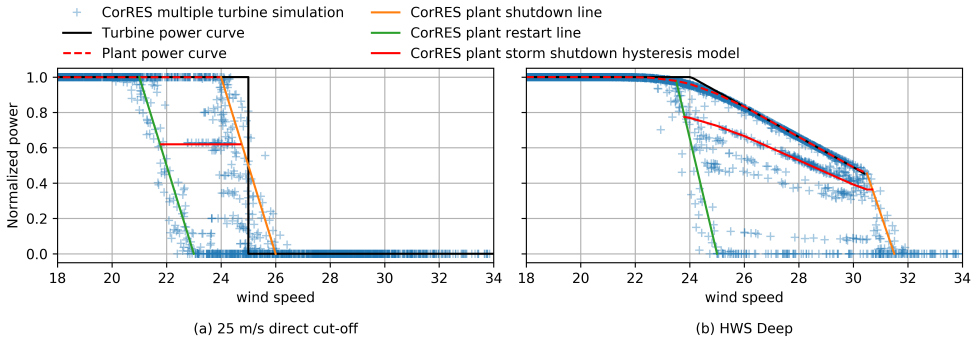


**Figure 5.** Plant vs single turbine storm shutdown for (a) 25 $\mathrm{ms}^{-1}$ direct cut-off (b) HWS deep. Multiple turbine simulations are aggregated in 5min. The shutdown hysteresis curve (in red) is an example case where restart occurs before the entire plant has shutdown.

### 3.3 Measured data for model validation and calibration

Four years of measured generation on 15 $\mathrm{min}$ resolution from 2015 to 2018 from the plants in BE2018 are used for model validation, see Fig. 3. Measured generation on 1 $\mathrm{min}$ resolution for 2018 is aggregated to 5 $\mathrm{min}$ resolution to validate the simulated 5 $\mathrm{min}$ ramps. The measured values with wind speed between 5 and 15 $\mathrm{ms}^{-1}$ and no power generation are classified as not available. Such data points were considered to be either measurement errors or indicating that the whole fleet is unavailable.

Wind speed nacelle anemometer measurements are available on the plants in BE2018 in 10 minute resolutions from 4 turbines in the corners of each plant. For comparison to CorRES simulations, the mean of the 4 turbines is taken to represent the effective wind speed of the plant and a fleet-level wind speed is defined by taking the weighted mean by installed capacity.

The wake model wake expansion parameter is calibrated in order to minimize the errors in predicting the capacity factors in the plants of BE2018 during the 2015-2018 period. The wake model calibration produces generation time series with consistent wake/blockage losses as observed in the measurements, but the model applies a constant wake expansion over the whole time series.

Model validation consists in comparing the temporal structure of the wind speed and power time series. A detail comparison is done in terms of wind speed and power production distributions, wind speed and power fluctuations distributions, and spatial correlation of power and power fluctuations.

## 4 Results for BE2018

Fig. 6 illustrates the wind speed fluctuation in 10 min measured and modelled with different approaches. This Fig. illustrates the need for adding fluctuations to the WRF datasets, and in particular, the need for non-Gaussian distributed fluctuations.

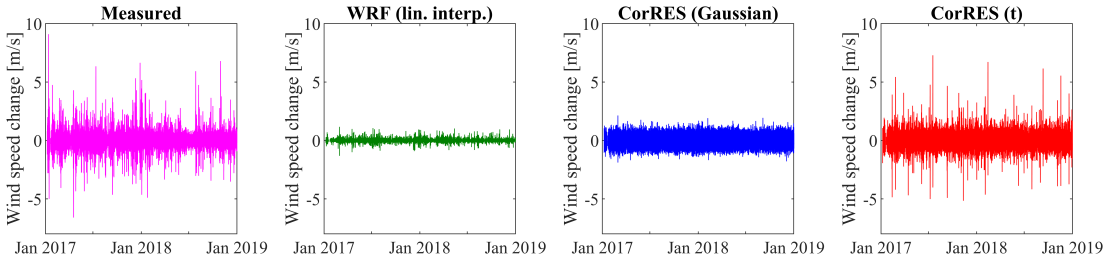


**Figure 6.** Wind speed fluctuations in 10min: measured, WRF, WRF with Gaussian fluctuations (CorRES(Gaussian)) and WRF with t-student Gaussian copula fluctuations (CorRES(t)).

Fig. 7 presents the qq-plot for the 10 min wind speed fluctuation on each of the plants in BE2018. It can be seen that the introduction of t-distributed fluctuations better represents the measured wind speed fluctuations. Table 2 presents the validation of extreme values of wind speed. It can be seen that WRF without fluctuations and without extreme correction factor (see eq. 9) under-predict the extreme wind speeds. The extreme values are better captured by CorRES; but due to the stochastic nature of the fluctuation model, many realizations of the time-series will need to be sampled to capture the maxima.

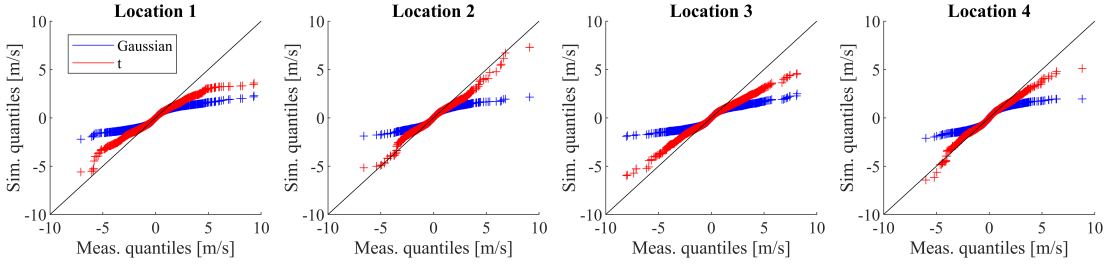


**Figure 7.** qq-plot of simulated vs measured wind speed fluctuation in 10min.

A comparison of the measured and modeled fleet-level (weighed average of individual plants by installed capacity) wind speed and power distributions of the BE2018 is depicted in Fig. 8. Note that the measured wind speeds include wake deficits (below 14 $\mathrm{ms}^{-1}$ ), while CorRES wind speed simulations are given without wake losses. CorRES considers the wakes in the plant power curve used to transform wind speed and wind direction to power. Despite this difference, it can be seen that the fleet

| Wind speed | Prct 99.9 | Prct 99.99 | Max |
|---|---|---|---|
| WRF | 22.8 | 25.4 | 26.2 |
| CorRES | 23.9 | 27.9 | 30.0 |
| Measured | 25.2 | 28.2 | 31.3 |

**Table 2.** Extreme (fleet-level mean) wind speed validation by comparing high percentiles (Prct) and maximum.

power production including the storm shutdown is accurately captured. The distribution of power production for measurements and CorRES, differ around rated power, because wind turbine availability is not modeled in CorRES.

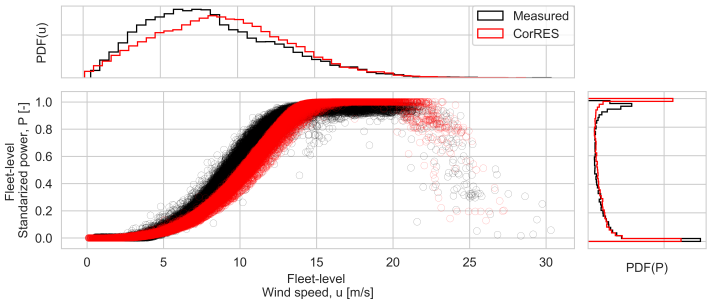


**Figure 8.** Measured and CorRES simulations of power vs wind speed, with their histograms for BE2018.

The validation of the spatial correlation of power production and power fluctuations is presented in Fig. 9. Note that CorRES is able to capture the spatial correlation trends: a decrease in correlation between the power of plants as a function of the distance between them. Similarly, the spatial correlation trend for the power ramps (fluctuations) is well reproduced by the simulations. This capability of simulating the spatial and temporal correlation between plants ensures accurate simulations of future installed capacity scenarios with different geographical installation distributions.

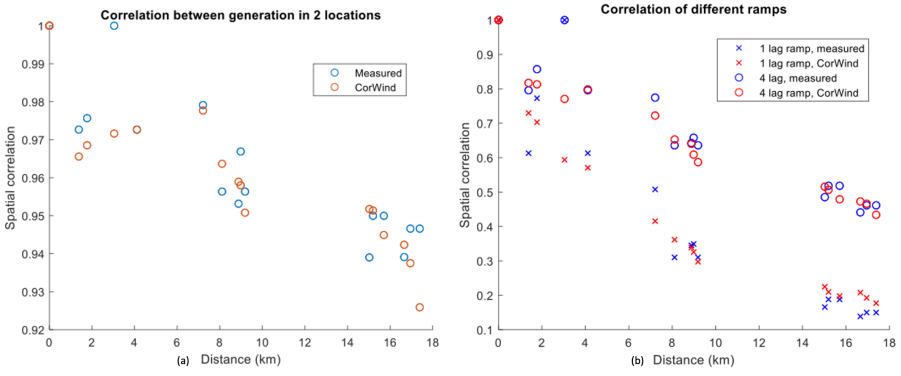


**Figure 9.** (a) Correlation of power production vs distance between two plants. (b) Correlation of power ramps vs distance between two plants for 15 min (1 lag) and 60 min (4 lag).

Model validation results in terms of capacity factors (CF), standard deviation of standardize production (SD) and standard deviation of different power fluctuation on different time windows (5min: DP5, 15min: DP15, 1h: DP60) are presented in table 3. The measured fleet CF is slightly over-predicted, this over-prediction becomes of 1.13% when a standard loss factor from un-availability (0.97) is applied. In this paper availability is not applied as a factor to the full time series in order to be conservative in the amount of full range power fluctuations.

| | Measured | CorRES | Residual | | Measured | CorRES | Residual |
|---|---|---|---|---|---|---|---|
| CF | 0.399 | 0.416 | 4.3% | SD_DP5 | 0.013 | 0.015 | 15.4 % |
| CF with availability | 0.399 | 0.404 | 1.1% | SD_DP15 | 0.033 | 0.032 | -3.0% |
| SD | 0.350 | 0.351 | 0.3% | SD_DP60 | 0.087 | 0.089 | 2.3% |
| Prct 1 DP5 | -0.040 | -0.043 | 7.5% | Prct 99 DP5 | 0.040 | 0.044 | 10.0% |
| Prct 1 DP15 | -0.099 | -0.091 | -8.1% | Prct 99 DP15 | 0.101 | 0.091 | -9.9% |
| Prct 1 DP60 | -0.255 | -0.249 | -2.4% | Prct 99 DP60 | 0.270 | 0.257 | -4.8% |
| Prct 0.1 DP5 | -0.089 | -0.078 | -1.2% | Prct 99.9 DP5 | 0.081 | 0.076 | -6.2 % |
| Prct 0.1 DP15 | -0.226 | -0.151 | -33.2% | Prct 99.9 DP15 | 0.205 | 0.156 | -23.9% |
| Prct 0.1 DP60 | -0.495 | -0.432 | -12.7% | Prct 99.9 DP60 | 0.511 | 0.429 | -16.0% |

**Table 3.** BE2018 residuals (prediction error) in capacity factor (CF), in standard deviation of standardised power (SD), standard deviation of 5, 15 and 60 min power fluctuations (DP5, DP15, DP60).

The distributions of different power fluctuation on different time windows (5min, 15min, 1h) are presented in Fig. 10. Over all, the distribution of the different power ramps are well captured by the model, besides the small differences on the tails. The difference in the tails is a combination of the lack of availability model in CorRES, the stochastic nature of the wind speed fluctuations models and the fact that only three years of measurements are available.

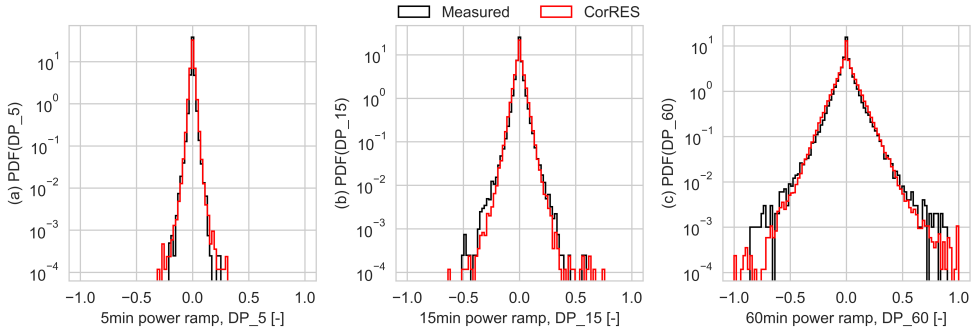


**Figure 10.** Distributions of standardized power fluctuations on different windows: (a) 5 min (DP_5), (b) 15 min (DP_15) and (c) 1h (DP_60).

## 5 Results for future fleet

Simulation results for 37 years of wind speed time series for the different scenarios (installed capacity, turbine technology and shutdown technology) in terms of CF, SD and standard deviation of power ramps (SD DP) are shown in table 4. The capacity

factor of the Belgian offshore wind fleet is expected to increase sequentially from BE 2018, to 2.3 GW, to the 4.4 GW fleet, due to the use of modern turbines with higher hub heights. A larger capacity factor is obtained when the technology B is used in the 4.4 GW fleet, while the deep storm shutdown technology only increases the CF marginally.

The standard deviation of the power shows an increase from BE 2018 to BE 2.3 GW scenarios due to the increased capacity factor, installed capacity, hub heights and to larger wake losses. In the 4.4 GW scenario, technology B shows a slightly larger SD than technology A due to the steeper power curve and larger hub heights; technology A does not increase SD with respect the 2.3 GW scenario.

The standard deviation of power ramps decrease from BE 2018 to 2.3 GW to 4.4 GW, due to the effect of geographical smoothing. There is no significant difference between the standard deviation of the power ramps among turbine or storm shutdown technologies.

| | | | CF | ratio CF | SD | ratio SD | SD DP5 | ratio SD DP5 | SD DP15 | ratio SD DP15 | SD DP60 | ratio SD DP60 |
|---|---|---|---|---|---|---|---|---|---|---|---|---|
| **BE 2018 (877 MW)** | | | 0.420 | 100% | 0.346 | 100% | 0.015 | 100% | 0.035 | 100% | 0.092 | 100% |
| **2.3 GW** | | | 0.430 | 103% | 0.354 | 102% | 0.013 | 81% | 0.031 | 88% | 0.088 | 96% |
| **4.4 GW** | **Tech A** | **25 m/s** | 0.449 | 107% | 0.354 | 102% | 0.011 | 69% | 0.026 | 74% | 0.079 | 86% |
| | | **Deep** | 0.450 | 107% | 0.355 | 102% | 0.010 | 67% | 0.026 | 74% | 0.078 | 85% |
| | **Tech B** | **25 m/s** | 0.485 | 116% | 0.357 | 103% | 0.011 | 70% | 0.027 | 76% | 0.080 | 87% |
| | | **Deep** | 0.488 | 116% | 0.358 | 103% | 0.010 | 68% | 0.026 | 74% | 0.078 | 85% |

**Table 4.** Capacity factors (CF), standard deviation of standardised power (SD), and standard deviations of power ramps in 5 min, 15 min and 60 min (SD DP5, SD DP15, SD DP60) and their relative ratios with respect BE 2018. All statistics are computed over the 37yrs of simulations.

Fig. 11 presents the comparison of the power fluctuations during low wind speeds (fleet-level weighted mean wind speed below 15 m/s) over the different installation/technology scenarios. The 4.4GWscenarios show the lowest variability of power fluctuations, followed by BE 2.3GWand BE 2018. These fluctuations are mainly caused by wind speed fluctuations and depend on the steepness of the power curve. The distribution of low wind speed ramps is symmetric because the power curve behaves almost linearly in this wind speed range.

Similarly, Fig. 12 shows the comparison of the power fluctuations during high wind speeds (fleet-level weighted mean wind speed larger than 15 m/s). The geographical smoothing and the high wind speed operation significantly reduce the tails (i.e. extreme events) of the power fluctuation distributions. The 2.3GW scenario shows a large reduction in the extreme power ramping with respect to BE 2018 because of the use of HWS storm protection technologies. Furthermore, all scenarios show non symmetric distributions with larger extreme positive ramps. Extreme negative ramps (at high wind speed) occur when the fleet shutdowns during a storm, while large positive ramps occur when the turbines restart after a shutdown during high wind speeds. In the 4.4 GW scenario, the 25 m/s direct cut-off shutdown shows the largest extreme power fluctuations for positive and negative ramps at high wind speed with a frequency of mid-range ramp events above the BE 2018 scenario, while BE 4.4 GW HWS deep shows the least extreme power fluctuations of all scenarios. The extreme positive ramps at high wind speeds

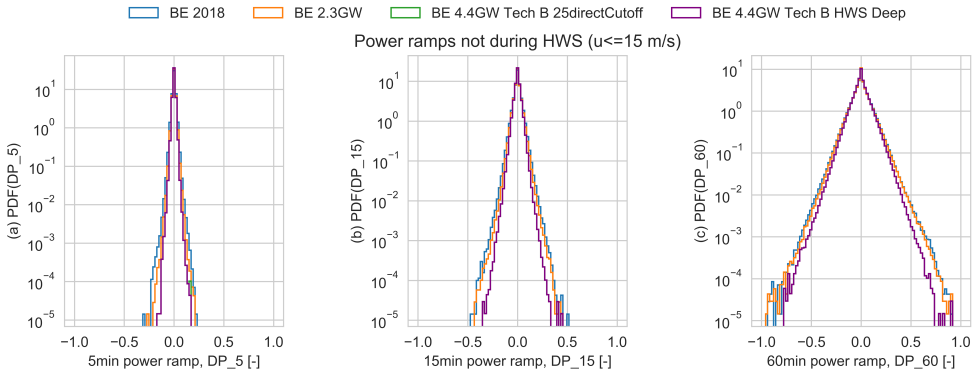


**Figure 11.** Distributions of standardized power fluctuations during low wind speeds in all the scenarios on different time windows: (a) 5 min (DP_5), (b) 15 min (DP_15) and (c) 1h (DP_60). The curves for the BE 4.4GW Tech B scenarios are on top of each other, with only a small difference in the left figure at around DP_5 = 0.2. Tech A is omitted for clarity because it behaves very similar to Tech B.

for BE 4.4 GW HWS deep and BE 2.3 GW are larger than the extreme negative ramps; these extreme positive ramps are a consequence of the turbine restart operation.

The extreme ramping events during low wind speeds are lower than the ramps at high wind speed for BE 2028 and BE 4.4 GW with 25 m/s direct cut-off. While the 2.3 GW and 4.4 GW with HWS deep scenarios show similar negative extreme power ramp values for low and high wind speeds.

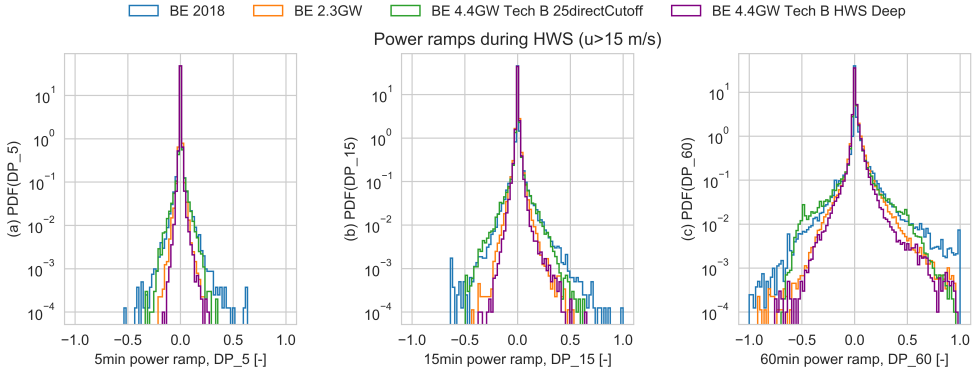


**Figure 12.** Distributions of standardized power fluctuations during high wind speeds in all the scenarios on different time windows: (a) 5 min (DP_5), (b) 15 min (DP_15) and (c) 1h (DP_60).

The extreme power ramps on different time windows for all scenarios (on all wind speeds) are summarized in table 5. There is a reduction in extreme ramps between the BE 2018 and 2.3 GW scenarios. In the 4.4 GW scenario, the HWS deep mitigates the extreme ramp events with respect both BE 2018 and 2.3 GW scenarios, while the reference direct cutoff shows an increase in extreme events. From table 4 it can be concluded that geographical distribution of installations has the major impact on the

general level of variability (standard deviation of power ramps), while tables 4 and 5 shows that the storm shutdown type only impacts the tails of the ramp distribution, especially for DP5 and DP15.

| DP5 | | | Prct. 0.01 | ratio Prct. 0.01 | Prct. 0.1 | ratio Prct. 0.1 | Prct. 99.9 | ratio Prct. 99.9 | Prct. 99.99 | ratio Prct. 99.99 |
|---|---|---|---|---|---|---|---|---|---|---|
| **BE 2018 (877 MW)** | | | -0.130 | 100.0% | -0.078 | 100.0% | 0.078 | 100.0% | 0.136 | 100.0% |
| **2.3 GW** | | | -0.097 | 74.6% | -0.061 | 78.2% | 0.063 | 80.8% | 0.097 | 71.3% |
| **4.4 GW** | **Tech A** | **25 m/s** | -0.102 | 78.5% | -0.050 | 64.1% | 0.052 | 66.7% | 0.098 | 72.1% |
| | | **Deep** | -0.072 | 55.4% | -0.048 | 61.5% | 0.050 | 64.1% | 0.075 | 55.1% |
| | **Tech B** | **25 m/s** | -0.110 | 84.6% | -0.054 | 69.2% | 0.054 | 69.2% | 0.107 | 78.7% |
| | | **Deep** | -0.076 | 58.5% | -0.050 | 64.1% | 0.050 | 64.1% | 0.079 | 58.1% |

| DP15 | | | Prct. 0.01 | ratio Prct. 0.01 | Prct. 0.1 | ratio Prct. 0.1 | Prct. 99.9 | ratio Prct. 99.9 | Prct. 99.99 | ratio Prct. 99.99 |
|---|---|---|---|---|---|---|---|---|---|---|
| **BE 2018 (877 MW)** | | | -0.268 | 100.0% | -0.171 | 100.0% | 0.178 | 100.0% | 0.291 | 100.0% |
| **2.3 GW** | | | -0.224 | 83.6% | -0.147 | 86.0% | 0.156 | 87.6% | 0.237 | 81.4% |
| **4.4 GW** | **Tech A** | **25 m/s** | -0.224 | 83.6% | -0.125 | 73.1% | 0.131 | 73.6% | 0.230 | 79.0% |
| | | **Deep** | -0.170 | 63.4% | -0.117 | 68.4% | 0.124 | 69.7% | 0.187 | 64.3% |
| | **Tech B** | **25 m/s** | -0.236 | 88.1% | -0.131 | 76.6% | 0.134 | 75.3% | 0.245 | 84.2% |
| | | **Deep** | -0.179 | 66.8% | -0.121 | 70.8% | 0.124 | 69.7% | 0.191 | 65.6% |

| DP60 | | | Prct. 0.01 | ratio Prct. 0.01 | Prct. 0.1 | ratio Prct. 0.1 | Prct. 99.9 | ratio Prct. 99.9 | Prct. 99.99 | ratio Prct. 99.99 |
|---|---|---|---|---|---|---|---|---|---|---|
| **BE 2018 (877 MW)** | | | -0.604 | 100.0% | -0.425 | 100.0% | 0.463 | 100.0% | 0.732 | 100.0% |
| **2.3 GW** | | | -0.561 | 92.9% | -0.395 | 92.9% | 0.434 | 93.7% | 0.629 | 85.9% |
| **4.4 GW** | **Tech A** | **25 m/s** | -0.541 | 89.6% | -0.366 | 86.1% | 0.393 | 84.9% | 0.600 | 82.0% |
| | | **Deep** | -0.489 | 81.0% | -0.343 | 80.7% | 0.375 | 81.0% | 0.544 | 74.3% |
| | **Tech B** | **25 m/s** | -0.537 | 88.9% | -0.380 | 89.4% | 0.397 | 85.7% | 0.588 | 80.3% |
| | | **Deep** | -0.503 | 83.3% | -0.354 | 83.3% | 0.374 | 80.8% | 0.553 | 75.5% |

**Table 5.** Extreme power ramps in 5 min, 15 min and 60 min and their relative ratios with respect BE2018.

## 6 Discussions

The increase in CF in the 4.4 GW scenario with wind turbine technology B is due to the larger rotor size and taller hub heights, but financial analysis may result in selections of turbines with less expensive rotors. Similarly, the 2.3 GW scenario showed a larger CF than BE 2018 because of the overall trend in increasing rotor sizes and taller tower, see table 1, this occurs even though there is an increase in wake losses due to the farm to farm interaction in BE 2.3 GW, see figure 3.

In general, the power fluctuation decrease in the 4.4 GW scenario. This is caused by the larger distances between plants, which causes a geographical smoothing due to lower correlation between the individual plant power time series. This results are consistent with the literature (Holttinen et al., 2016; Koivisto et al., 2016, 2019b, 2020).

There is a trend to have the most extreme power fluctuations occur during high wind, such that it is possible to lose 75% of the installed capacity in one hour during an extreme storm event. But the use of modern high wind speed operation technologies mitigates the impact of extreme down-ramps to the point that similar extreme down-ramp events are seen at low and high wind speeds. Extreme up-ramps are more likely to occur than similar size down ramps, because the wind turbine storm shutdown

345 technologies only mitigate the shutdowns and not the restart part of the power curve. Mitigation of such up-ramp events (during and after storms) should be addressed as they represent some of the largest power fluctuation events.

The extreme ramping events at low wind speeds become equally important as the high wind speed extreme ramps when turbines with modern high wind speed operation are installed. This means that mitigation approaches that operate at both high and low wind speeds are needed to further reduce power fluctuations. Geographical location of installations has a major impact
350 on the standard deviation of power ramps and therefore it can be used for further mitigation of power fluctuations.

Even though the t-distribution wind speed fluctuations was deemed necessary to accurately capture the power fluctuations, a more theoretically sound modeling approach could consists in a stochastic model with non-stationary Gaussian wind speed fluctuations, in which the variance is a function of the stability and turbulence intensity time series. These additional variables are available in some of the weather models.

355 Improved wake modelling could also be implemented in the presented approach. The use of computational fluid dynamics Reynolds averaged (RANS) wake models such as (van der Laan et al., 2015) has been proven to be more accurate to predict not only wake losses but also losses due to blockage effects (Bleeg et al., 2018), and therefore produce more accurate generation time series. Due to the large size of the Belgian-Dutch fleet, such simulations were not possible in the present study. Another possible improvement of the wake modeling is to consider stability dependent plant power curves, this means that the power
360 time series will be interpolated using the wind speed, wind direction and stability time series. Additional improvements in the inclusion of wind turbine dynamics could open the possibility to make simulations in higher time resolution, but such models were considered out of scope for this study.

To further reduce the conservatism of the present analysis a stochastic availability model should be developed. This will remove the discrepancy between the distribution of fleet-level wind power production seen at around rated power. Nevertheless,
365 the proposed methodology successfully represented the fleet-level ramp distributions as compared with the measured data.

## 7 Conclusions

The model validation shows that the methodology presented in this paper is able to capture the distribution of fleet-level wind speed and power production, while at the same time capturing the main spatio-temporal characteristics of the time series. The t-student and extreme wind speed corrections improved the accuracy of simulated extreme events in the wind speed and power
370 fluctuation distributions. The hysteresis plant storm shutdown model is able to capture the modern high wind speed operation technologies offered by the main turbine manufacturers. The use of a long time series (37 years) of generation is fundamental in order to quantify the likelihood of the extreme fleet-level power fluctuations.

The future 4.4 GW fleet has an increased capacity factor while at the same time shows a reduction in the standardized power fluctuations with respect the 2.3 GW fleet. However, for the high wind speed events, a reduction of the extreme power
375 ramps is only achievable with the use of modern high wind speed operation. Turbines with high wind speed operation affect the business case of a project by a marginal increase of the CF and a reduction of the imbalance costs, while at the same time this type of extended range operation makes the turbines more expensive. This means that the imbalance prices should be set

to give a financial incentive to the developers to select such technologies. On the energy system level, these technologies are crucial for extreme ramp event mitigation in cases where there is a tightly packed wind power fleet. The most extreme power fluctuations occur in the up-ramp, i.e. in the restart after shutdown, which can be mitigated by controlling the restart. This could be implemented in the turbine level by implementing a gradual restart curve or on the system level by forcing the plants to come back to power in a gradual manner.

The extreme ramping events at low wind speeds become equally important as at high wind speeds when modern high wind speed operation is installed in the fleet. This means that approaches that operate at both high and low wind speeds are needed to achieve further reductions of power fluctuations. Geographical distribution of installations has the major impact on reducing the standard deviation of power ramps, therefore plant-to-plant distance should be considered to further mitigate power fluctuations.

The methodology and analysis presented in this paper are relevant for the future offshore installations in the North Sea. It is expected that countries like Germany and United Kingdom will reach similar density of offshore installation as there is currently in Belgium (Agora Energiewende et al., 2020).

*Code and data availability.* The data and code presented in this paper are not publicly available.

*Author contributions.* Juan Pablo Murcia and Matti Koivisto are responsible for writing the article, model development, simulations and analysis. Poul Sørensen and Philipe Magnant are responsible for supervision and comments.

*Competing interests.* The authors report that there is no conflict of interests in this study.

*Acknowledgements.* The authors would like to thank the wind plant operators for providing data. Elia, ForskEL/EUDP OffshoreWake project (PSO-12521) and DTU Wind Energy (PSfuture) for supporting the model development.

## References


Agora Energiewende, Agora Verkehrswende, Technical University of Denmark, and Max-Planck-Institute for Biogeochemistry: Making the Most of Offshore Wind: Re-Evaluating the Potential of Offshore Wind in the German North Sea, Tech. rep., 2020.

Apt, J.: The spectrum of power from wind turbines, Journal of Power Sources, 169, 369–374, 2007.

Bastankhah, M. and Porté-Agel, F.: A new analytical model for wind-turbine wakes, Renewable Energy, 70, 116–123, 2014.

Bastine, D., Larsén, X., Witha, B., Dörenkämper, M., and Gottschall, J.: Extreme winds in the New European Wind Atlas, in: Journal of Physics: Conference Series, vol. 1102, p. 012006, IOP Publishing, 2018.

Bleeg, J., Purcell, M., Ruisi, R., and Traiger, E.: Wind farm blockage and the consequences of neglecting its impact on energy production, Energies, 11, 1609, 2018.

Buijs, P., Bekaert, D., Van Hertem, D., and Belmans, R.: Needed investments in the power system to bring wind energy to shore in Belgium, in: 2009 IEEE Bucharest PowerTech, pp. 1–6, IEEE, 2009.

Danish Energy Agency: Technology Catalogue, 2020, Tech. rep., 2020.

Dee, D. P., Uppala, S. M., Simmons, A., Berrisford, P., Poli, P., Kobayashi, S., Andrae, U., Balmaseda, M., Balsamo, G., Bauer, d. P., et al.: The ERA-Interim reanalysis: Configuration and performance of the data assimilation system, Quarterly Journal of the royal meteorological society, 137, 553–597, 2011.

Ekström, J., Koivisto, M., Mellin, I., Millar, R. J., and Lehtonen, M.: A statistical model for hourly large-scale wind and photovoltaic generation in new locations, IEEE Transactions on Sustainable Energy, 8, 1383–1393, 2017.

Elia, B. T. S. O.: Electricity Scenarios for Belgium towards 2050, Tech. rep., 2017.

Elia, B. T. S. O.: Offshore Integration Study, Tech. rep., 2018.

Elia, B. T. S. O.: Adequacy and flexibility study for Belgium 2020-2030, Tech. rep., 2019.

Engeland, K., Borga, M., Creutin, J.-D., François, B., Ramos, M.-H., and Vidal, J.-P.: Space-time variability of climate variables and intermittent renewable electricity production–A review, Renewable and Sustainable Energy Reviews, 79, 600–617, 2017.

Fertig, E.: Simulating subhourly variability of wind power output, Wind Energy, 22, 1275–1287, 2019.

Gelaro, R., McCarty, W., Suárez, M. J., Todling, R., Molod, A., Takacs, L., Randles, C. A., Darmenov, A., Bosilovich, M. G., Reichle, R., et al.: The modern-era retrospective analysis for research and applications, version 2 (MERRA-2), Journal of Climate, 30, 5419–5454, 2017.

González-Aparicio, I., Monforti, F., Volker, P., Zucker, A., Careri, F., Huld, T., and Badger, J.: Simulating European wind power generation applying statistical downscaling to reanalysis data, Applied Energy, 199, 155–168, 2017.

Hersbach, H., Bell, B., Berrisford, P., Hirahara, S., Horányi, A., Muñoz-Sabater, J., Nicolas, J., Peubey, C., Radu, R., Schepers, D., et al.: The ERA5 global reanalysis, Quarterly Journal of the Royal Meteorological Society, 2020.

Holttinen, H., Meibom, P., Orths, A., Lange, B., O'Malley, M., Tande, J. O., Estanqueiro, A., Gomez, E., Söder, L., Strbac, G., et al.: Impacts of large amounts of wind power on design and operation of power systems, results of IEA collaboration, Wind Energy, 14, 179–192, 2011.

Holttinen, H., Lemstrom, B., Meibom, P., Bindner, H., Orths, A., Van Hulle, F., Ensslin, C., Tiedemann, A., Hofmann, L., Winter, W., et al.: Design and operation of power systems with large amounts of wind power: state of the art report, 2016.

Huber, M., Dimkova, D., and Hamacher, T.: Integration of wind and solar power in Europe: Assessment of flexibility requirements, Energy, 69, 236–246, 2014.

Kiviluoma, J., Holttinen, H., Weir, D., Scharff, R., Söder, L., Menemenlis, N., Cutululis, N. A., Danti Lopez, I., Lannoye, E., Estanqueiro, A., et al.: Variability in large-scale wind power generation, Wind Energy, 19, 1649–1665, 2016.

Klöckl, B. and Papaefthymiou, G.: Multivariate time series models for studies on stochastic generators in power systems, Electric Power Systems Research, 80, 265–276, 2010.

Koivisto, M., Ekström, J., Seppänen, J., Mellin, I., Millar, J., and Haarla, L.: A statistical model for comparing future wind power scenarios with varying geographical distribution of installed generation capacity, Wind Energy, 19, 665–679, 2016.

Koivisto, M., Das, K., Guo, F., Sørensen, P., Nuño, E., Cutululis, N., and Maule, P.: Using time series simulation tools for assessing the effects of variable renewable energy generation on power and energy systems, Wiley Interdisciplinary Reviews: Energy and Environment, 8, e329, 2019a.

Koivisto, M., Maule, P., Cutululis, N., and Sørensen, P.: Effects of Wind Power Technology Development on Large-scale VRE Generation Variability, in: 2019 IEEE Milan PowerTech, pp. 1–6, IEEE, 2019b.

Koivisto, M., Jónsdóttir, G. M., Sørensen, P., Plakas, K., and Cutululis, N.: Combination of meteorological reanalysis data and stochastic simulation for modelling wind generation variability, Renewable Energy, 2020.

Larsén, X. G. and Kruger, A.: Application of the spectral correction method to reanalysis data in South Africa, Journal of wind engineering and industrial aerodynamics, 133, 110–122, 2014.

Larsén, X. G., Ott, S., Badger, J., Hahmann, A. N., and Mann, J.: Recipes for correcting the impact of effective mesoscale resolution on the estimation of extreme winds, Journal of Applied Meteorology and Climatology, 51, 521–533, 2012.

Larsén, X. G., Larsen, S. E., and Petersen, E. L.: Full-scale spectrum of boundary-layer winds, Boundary-layer meteorology, 159, 349–371, 2016.

Leahy, P. G. and Foley, A. M.: Wind generation output during cold weather-driven electricity demand peaks in Ireland, Energy, 39, 48–53, 2012.

Litong-Palima, M., Bjerge, M. H., Cutululis, N. A., Hansen, L. H., and Sørensen, P.: Modeling of the dynamics of wind to power conversion including high wind speed behavior, Wind Energy, 19, 923–938, 2016.

Liu, H., Jin, Y., Tobin, N., and Chamorro, L. P.: Towards uncovering the structure of power fluctuations of wind farms, Physical Review E, 96, 063 117, 2017.

Liu, Y., Warner, T., Liu, Y., Vincent, C., Wu, W., Mahoney, B., Swerdlin, S., Parks, K., and Boehnert, J.: Simultaneous nested modeling from the synoptic scale to the LES scale for wind energy applications, Journal of Wind Engineering and Industrial Aerodynamics, 99, 308–319, 2011.

Macdonald, H., Hawker, G., and Bell, K.: Analysis of wide-area availability of wind generators during storm events, in: 2014 International Conference on Probabilistic Methods Applied to Power Systems (PMAPS), pp. 1–6, IEEE, 2014.

Marinelli, M., Maule, P., Hahmann, A. N., Gehrke, O., Nørgrd, P. B., and Cutululis, N. A.: Wind and photovoltaic large-scale regional models for hourly production evaluation, IEEE Transactions on Sustainable Energy, 6, 916–923, 2014.

Mehrens, A. R., Hahmann, A. N., Larsén, X. G., and von Bremen, L.: Correlation and coherence of mesoscale wind speeds over the sea, Quarterly Journal of the Royal Meteorological Society, 142, 3186–3194, 2016.

Mikova, N., Eichhammer, W., and Pfluger, B.: Low-carbon energy scenarios 2050 in north-west European countries: Towards a more harmonised approach to achieve the EU targets, Energy policy, 130, 448–460, 2019.

Nuño, E., Maule, P., Hahmann, A., Cutululis, N., Sørensen, P., and Karagali, I.: Simulation of transcontinental wind and solar PV generation time series, Renewable Energy, 118, 425–436, 2018.

Olauson, J.: ERA5: The new champion of wind power modelling?, Renewable energy, 126, 322–331, 2018.

Olauson, J. and Bergkvist, M.: Modelling the Swedish wind power production using MERRA reanalysis data, Renewable Energy, 76, 717–725, 2015.

Olauson, J., Bergström, H., and Bergkvist, M.: Restoring the missing high-frequency fluctuations in a wind power model based on reanalysis data, Renewable energy, 96, 784–791, 2016.

Olauson, J., Bergkvist, M., and Rydén, J.: Simulating intra-hourly wind power fluctuations on a power system level, Wind Energy, 20, 973–985, 2017.

Pfenninger, S.: Dealing with multiple decades of hourly wind and PV time series in energy models: A comparison of methods to reduce time resolution and the planning implications of inter-annual variability, Applied energy, 197, 1–13, 2017.

Pfenninger, S., Hawkes, A., and Keirstead, J.: Energy systems modeling for twenty-first century energy challenges, Renewable and Sustainable Energy Reviews, 33, 74–86, 2014.

Porté-Agel, F., Bastankhah, M., and Shamsoddin, S.: Wind-turbine and wind-farm flows: a review, Boundary-Layer Meteorology, 174, 1–59, 2020.

Roques, F., Hiroux, C., and Saguan, M.: Optimal wind power deployment in Europe—A portfolio approach, Energy policy, 38, 3245–3256, 2010.

Santos-Alamillos, F., Thomaidis, N., Usaola-García, J., Ruiz-Arias, J., and Pozo-Vázquez, D.: Exploring the mean-variance portfolio optimization approach for planning wind repowering actions in Spain, Renewable Energy, 106, 335–342, 2017.

Skamarock, W. C., Klemp, J. B., Dudhia, J., Gill, D. O., Barker, D. M., Wang, W., and Powers, J. G.: A description of the Advanced Research WRF version 3. NCAR Technical note-475+ STR, 2008.

Sørensen, P., Hansen, A. D., and Rosas, P. A. C.: Wind models for simulation of power fluctuations from wind farms, Journal of wind engineering and industrial aerodynamics, 90, 1381–1402, 2002.

Sørensen, P., Cutululis, N. A., Vigueras-Rodríguez, A., Madsen, H., Pinson, P., Jensen, L. E., Hjerrild, J., and Donovan, M.: Modelling of power fluctuations from large offshore wind farms, Wind Energy: An International Journal for Progress and Applications in Wind Power Conversion Technology, 11, 29–43, 2008.

Sørensen, P., Litong-Palima, M., Hahmann, A. N., Heunis, S., Ntusi, M., and Hansen, J. C.: Wind power variability and power system reserves in South Africa, Journal of Energy in Southern Africa, 29, 59–71, 2018.

Sørensen, P., Koivisto, M., and Murcia, J.: Elia - MOG II System Integration: Public version, no. E-0203 in DTU Wind Energy E, DTU Wind Energy, Denmark, 2020.

Staffell, I. and Pfenninger, S.: Using bias-corrected reanalysis to simulate current and future wind power output, Energy, 114, 1224–1239, 2016.

Staffell, I. and Pfenninger, S.: The increasing impact of weather on electricity supply and demand, Energy, 145, 65–78, 2018.

Talbot, C., Bou-Zeid, E., and Smith, J.: Nested mesoscale large-eddy simulations with WRF: Performance in real test cases, Journal of Hydrometeorology, 13, 1421–1441, 2012.

Tejeda, C., Gallardo, C., Domínguez, M., Gaertner, M. Á., Gutierrez, C., and de Castro, M.: Using wind velocity estimated from a reanalysis to minimize the variability of aggregated wind farm production over Europe, Wind Energy, 21, 174–183, 2018.

Thomaidis, N. S., Santos-Alamillos, F. J., Pozo-Vázquez, D., and Usaola-García, J.: Optimal management of wind and solar energy resources, Computers & Operations Research, 66, 284–291, 2016.

van der Laan, M. P., Sørensen, N. N., Réthoré, P.-E., Mann, J., Kelly, M. C., Troldborg, N., Hansen, K. S., and Murcia, J. P.: The k--fP model applied to wind farms, Wind Energy, 18, 2065–2084, 2015.

Veers, P. S.: Three-dimensional wind simulation, Tech. rep., Sandia National Labs., Albuquerque, NM (USA), 1988.

Volker, P. J., Hahmann, A. N., Badger, J., and Jørgensen, H. E.: Prospects for generating electricity by large onshore and offshore wind farms, Environmental Research Letters, 12, 034 022, 2017.

Von Bremen, L.: Large-scale variability of weather dependent renewable energy sources, in: Management of weather and climate risk in the energy industry, pp. 189–206, Springer, 2010.